Journal of Volcanology and Geothermal Research 261 (2013) 316–329

Contents lists available at SciVerse ScienceDirect

Journal of Volcanology and Geothermal Research

journal homepage: www.elsevier.com/locate/jvolgeores

The Merapi 2010 eruption: An interdisciplinary impact assessment methodology for studying pyroclastic density current dynamics

S. Jenkins [a,*], J.-C. Komorowski [b], P.J. Baxter [c], R. Spence [a], A. Picquout [d], F. Lavigne [d], Surono [e]

[a] Cambridge Architectural Research, Unit 6, 25 Gwydir Street, Cambridge, CB1 2LG, UK
[b] Equipe de Géologie des Systèmes Volcaniques, Institut de Physique du Globe de Paris, Sorbonne Paris-Cité, Université René Diderot, CNRS UMR 7154, 1 Rue Jussieu, 75238 Paris Cedex 05, France
[c] Institute of Public Health, University of Cambridge, Robinson Way, Cambridge CB2 2SR, UK
[d] Paris 1 Pantheon-Sorbonne University, Laboratory of Physical Geography, Geography, Meudon, France
[e] Centre of Volcanology and Geological Hazard Mitigation (CVGHM), Jalan Diponegoro 57, 40122 Bandung, Indonesia

ARTICLE INFO

Article history:
Received 29 February 2012
Accepted 12 February 2013
Available online 27 February 2013

Keywords:
Pyroclastic density currents
Merapi volcano
Eruption impacts
Volcanic risk assessment
Interdisciplinary
Impact assessment

ABSTRACT

The large explosive eruption of Merapi volcano, Indonesia, in 2010 presented a key, and rare, opportunity to study the impacts of a major explosive eruption in a densely populated area. Pyroclastic density currents (PDCs) produced throughout the 2010 eruption were unusually destructive, causing near complete devastation across a 22 km^2 swath of the densely populated southern flanks and casualties to the end of their runout at 15.5 km from the volcano. The majority (>120) of the more than 200 fatalities occurred more than 12 km from the volcano, where many people were caught in PDCs as they were evacuating. The 2010 eruption (VEI 4) exhibited a range of PDC behaviour in a complex multi-stage event that marked a change in eruption behaviour at Merapi, being the first eruption of this magnitude and style since 1872. This shift in style may mark a change in regime, and so understanding the potential impact of such large explosive eruptions is essential for future risk-assessment at Merapi. We describe a new impact assessment methodology that allowed us to collect important empirical geological, damage and casualty information and reconstruct impact dynamics associated with the PDCs. In contrast to previous PDC impact studies, we combined remote, field, laboratory and GIS assessments and were able to enter the affected areas safely and before their disturbance by rains or human activity. By integrating the results of our geological, damage and medical studies, we could reconstruct the spatial and temporal dynamics of the PDCs and their main hazard characteristics. Our interdisciplinary methods and preliminary findings are discussed here. In the areas damaged by PDCs, we used empirical damage data and calculations of material and structural resistance to lateral force to estimate approximate dynamic pressures. Dynamic pressures associated with the 5 November paroxysm exceeded 15 kPa more than 6 km from source and rapidly attenuated over a distance of less than 1 km at the end of the PDC runouts. Analysis of thermal indicators, such as deformed plastic, and correlation with information on burns injuries and fires provided estimates of ambient temperatures associated with the PDCs. Even at the relatively low temperatures estimated for the PDCs (200–300 °C) they were lethal to people inside as well as outside buildings, in part because of the building design that enabled the PDCs to rapidly infiltrate inside. Such detailed quantitative data can be used to support numerical PDC and impact modelling and risk assessment at dome-forming volcanoes, providing an improved understanding of the complexity of PDCs and their associated impacts on exposed populations.

1. Introduction

Population growth and increasing urbanisation in areas of active volcanism require innovations in the development and implementation of risk assessments and mitigation measures if the potential for significant loss of life in major explosive eruptions is to be avoided (Baxter et al., 2008). However, major explosive volcanic eruptions in populated areas are rare and our understanding of their potential impacts lacking. The eruption of Merapi volcano in 2010 therefore presented a key opportunity to study the impacts of a major explosive eruption in a densely populated area. In particular, the eruption was characterised by a wide range of concentrated pyroclastic flows and dilute pyroclastic surges — Pyroclastic Density Currents (PDCs) — which are some of the most complex, destructive and least predictable volcanic processes and which were responsible for the majority of casualties and damage during the 2010 eruption. We have undertaken an interdisciplinary impact assessment of the eruption, which

* Corresponding author at: Department of Earth Sciences, University of Bristol, Bristol, BS8 1RJ, UK. Tel: +44 117 9545400; fax: +44 117 9253385.
E-mail addresses: susanna.Jenkins@gmail.com (S. Jenkins), komorow@ipgp.fr (J.-C. Komorowski), pjb21@medschl.cam.ac.uk (P.J. Baxter), robin.spence@carltd.com (R. Spence), adripicou@yahoo.fr (A. Picquout), franck.lavigne@univ-paris1.fr (F. Lavigne), surono@vsi.esdm.go.id (Surono).

0377-0273/$ – see front matter © 2013 Elsevier B.V. All rights reserved.
http://dx.doi.org/10.1016/j.jvolgeores.2013.02.012

is unique in the study of PDCs and their impacts on people and their environment because we were able to safely start our field investigation of the damage zone within three weeks of the eruption ending. In this paper, we describe the novel methods we developed as part of the assessment, our preliminary findings and the key perspectives they provide for quantifying impact dynamics associated with PDCs emplaced over multiple eruption stages at Merapi.

1.1. Background

Merapi volcano in Java, Indonesia, is one of the most active and densely populated volcanoes in the world, with the steep vegetated slopes home to more than one million people (Thouret et al., 2000). Eruptions over the last century have been characterised by relatively small dome growth and collapse events (VEI 0–3) producing 'Merapi-type' PDCs that rarely travelled more than 10 km from source (Voight et al., 2000). By contrast, the 2010 eruption (VEI 4) exhibited a range of PDC behaviour in a complex multi-stage event that marked a change in eruption style and behaviour, being the first eruption of this magnitude and style since 1872. It is not clear if this change in style marks a temporary or prolonged regime change and so understanding the potential impact of such large explosive eruptions at Merapi is essential for future risk-assessment.

The Merapi 2010 eruption rapidly escalated over a period of 11 days from 26 October towards a devastating paroxysm on 5 November, which threatened communities more than 15 km from the summit. Subsequent short-lived rapid dome growth from 5 to 8 November was followed by a decline in activity to eruption end on 23 November (Table 1). Prior to and during the 2010 eruption, more than 400,000 people were rapidly evacuated to official emergency shelters (Surono et al., 2012), with more than 1 million displaced from their homes (Lavigne et al., 2011). As a direct consequence of PDCs during the eruption more than 2200 buildings were damaged and over 200 people killed; a further 196 were officially attributed to being indirectly caused by the eruption, for example from vehicle accidents (Indonesian National Disaster Management Agency (BNPB), 12 December 2010). The eruption comprised eight main stages of activity (Table 1), of which four are pertinent to PDC impact assessment (dates and times are local: UTC + 7 h):

- An initial phreatomagmatic vent-clearing stage in which 34 people who refused to evacuate were killed and 4 injured, with more than 150 buildings damaged across an area of approximately 7.5 km^2 (Stage 2: 26 October 2010);
- An escalating stage of rapid dome growth and collapse with PDCs of increasing runout reaching to 12 km (Stage 3: 29 October to 4 November);
- Explosion of the dome and upper sealed conduit with associated laterally directed high-energy PDCs that felled trees and damaged more than 1300 buildings within a 22 km^2 sector of the south flank, producing block-rich channelised PDCs that reached more than 15 km from the crater (Stage 4: 00:02 to 00:13, 5 November);
- Retrogressive collapse of the remaining dome and upper edifice producing PDCs that reached 15.5 km from the crater, with concentrated PDC overspills and dilute detached PDCs extending up to 200 m from the channelised parent PDC and killing more than 120 people (Stage 5: 00:13 to 01:57, 5 November).

Empirical eruption impact data from areas affected by these PDCs, which includes geological, damage and casualty information collected as part of this study, are invaluable as they allow reconstruction and improved understanding of the PDC emplacement behaviour, dynamics and damaging mechanisms. Such data can also inform the relationships between deposits, volcanic processes and the damage sustained by people, buildings and infrastructure, which can be useful in vulnerability studies and planning for future crises. Continuing research into planning for and mitigating the impacts of future explosive volcanic eruptions in populated areas is multi-disciplinary by requirement: empirical impact data are therefore critical in

Table 1
Summary of the Merapi 2010 eruption phenomena with associated impacts (all dates and times are local, UTC + 7 h, and distances reported are radial). Eruptive activity at Merapi in 2010 began on 26 October after more than one year of unrest and precursory activity (Stage 1) and the eruption ended with short-lived rapid dome growth from 5 to 8 November where no impacts were incurred but there remained a potential for dome explosion or collapse (Stage 7) and sustained degassing and ash emission that declined from 8 through to 23 November with no major impact (Stage 8). More details can be found in the Bulletin of the Global Volcanism Network (2011) and Surono et al. (2012).

Stage	Dates/times	Stage activity	Phenomena	Spatial extent	Impact
2	26 to 29 October [3 days]	Initial phreatomagmatic vent-clearing	Laterally-directed explosion of a rapidly emplaced gaseous shallow cryptodome producing at least eight periods of PDC emplacement	Channelised PDCs to 6.8 km and 5.4 km in the Gendol and Kuning rivers to the south respectively and dilute unconfined PDCs across a 7.5 km^2 swath to the south	34 people who refused to evacuate killed by PDCs, 4 survive; ca. 150 buildings damaged; Strongly directional tree blowdown.
3	29 October to 4 November [7 days]	Escalating stage of rapid dome growth, recurrent dome explosions and dome collapse	PDCs of increasing frequency and runout directed to the south and mostly confined to the Gendol valley, with associated dilute PDCs to the south and southwest	PDCs to 3.5 km on 30 October (2 PDCs) to 9 km on 1 November (7 PDCs), 10 km on 3 November (38 PDCs) and 12 km on 4 November (continuous PDC activity)	Close-range seismic stations saturated by intense tremor (3 November); Partial PDC overspill damaged at least three recently evacuated villages.
4	00:02 to 00:13 5 November [11 min]	Explosion of the dome and upper sealed conduit	Laterally directed explosion and collapse with turbulent and block-rich channelised PDCs towards the south	Turbulent dilute PDCs across 22 km^2 sector on the south flank; concentrated channelised PDCs to 15.5 km in the Gendol valley	Few reported proximal casualties; >1200 buildings damaged or destroyed (includes buildings also damaged 26 October); Tens of thousands of trees felled and uprooted.
5	00:13 to 01:57 5 November [1 h, 44 min]	Retrogressive collapse of the remaining dome and upper edifice	Channelised PDCs with partial overspill	Maximum runout to 15.5 km in the Gendol valley, with concentrated PDC overspill and dilute detached PDCs extending up to 200 m from the parent channelised PDC	>120 people killed from PDC overspill along the Gendol 10–15 km from the volcano [a]; A further ~1000 buildings damaged or destroyed; Further damage to vegetation in overspill areas.
6	02:11 to 04:21 5 November [2 h, 10 min]	Fountain and subplinian convective column collapse	Scoria- and pumice-rich confined concentrated PDCs	Scoria-rich PDC to 13 km and pumice-rich PDC to 15 km in the Gendol valley.	Occasional overspill into adjacent villages with undefined impact because of previous inundation.

[a] It is difficult to distinguish casualties associated with PDC overspill between stages 4, 5 and 6 as they occurred within hours of each other and in certain villages there were multiple impacts.

reducing epistemic uncertainty surrounding complex PDC behaviour and impacts and providing information for a larger risk assessment framework, which includes numerical modelling and formalised risk analyses approaches such as expert elicitation (Aspinall, 2006).

1.2. Previous eruption impact assessments

Previous eruptions at Merapi have been considerably smaller and less destructive than the 2010 eruption but field studies associated with the 1994 and 2006 eruptions in particular provide important insight into PDC impacts at Merapi. Geological studies of PDC generation and emplacement during the 1994 eruption of Merapi (Abdurachman et al., 2000) can be considered alongside studies of the thermal and mechanical damage to plastics (Voight and Davis, 2000) and trees (Clarke and Voight, 2000; Kelfoun et al., 2000) to reconstruct approximate PDC peak emplacement temperatures (250 °C–350 °C: Voight and Davis, 2000) and velocities (~50 m/s: Kelfoun et al., 2000) for dilute PDCs impacting Turgo hill, 5.5 km southwest of the volcano and where a number of casualties were sustained. Following the 2006 eruption, separate studies of the geological characteristics of dense PDCs (Charbonnier and Gertisser, 2008) and their impacts on infrastructure (Wilson et al., 2007) were carried out, with Charbonnier and Gertisser using geological evidence and the melting of plastics to estimate, respectively, PDC temperatures (>165 °C) and velocities (24 m/s) in areas of Kaliadem 5.5 km south of the volcano and affected by dilute detached PDCs.

The destructive eruption of Mount St Helens in a forested wilderness area in 1980 provided a key turning point in volcanology, with impact studies offering scientific insight into PDC dynamics (Lipman and Mullineaux, 1981). However, few quantitative PDC impact studies of destructive high-energy PDCs affecting populated areas, as occurred at Merapi in 2010, have been carried out, principally due to the rarity of major explosive eruptions impacting human settlements. Notable exceptions include those following the eruptions of Mt Pelée in 1902 (Lacroix, 1904), Mt Lamington in 1953 (Taylor, 1958) and Soufrière Hills Volcano in 1997 (Baxter et al., 2005), which we describe briefly here.

Lacroix arrived in Martinique six weeks after the initial PDCs of 8 May 1902 struck St Pierre town causing partial destruction of robust masonry buildings and 28,000 deaths. The first scientific team in the impacted area (Kennan, 1902) arrived one day after the 20 May 1902 PDC, which had caused further damage in St Pierre. The only data available to show the impact of the initial 8 May PDC are photographs and associated damage descriptions provided in Lacroix's monograph (Lacroix, 1904), although Lacroix did not arrive until 21 June. Lacroix's landmark study was the first to estimate dynamic pressures and temperatures and to understand the very existence of dilute and highly mobile PDCs (surges) and their destructive potential in cities (including speculating on the destruction of Pompeii and Herculaneum by PDCs in the AD 79 eruption of Vesuvius).

Damage associated with the 21 January 1951 eruption of Mt Lamington in Papua New Guinea was documented by Taylor (1958); however, with the exception of buildings near the edge of the impact zone, 10–12 km north of the volcano, impacted buildings were timber frame and offered little resistance to, and therefore little information regarding, the thermal and pressure impacts in non-peripheral zones. However, Taylor again estimated temperatures and dynamic pressures where he could find evidence.

The building damage assessment carried out by Baxter et al. (2005) for three PDC events at Soufrière Hills Volcano, Montserrat, in 1997 utilised extensive photographs taken by helicopter and, because of the volcanic hazard, a short (three day) field mission in the area of the Boxing Day high-energy PDC between eight and thirteen months after the initial impacts. The areas remained evacuated from before impact until their assessment hence the area was not disturbed by human activity, although inevitably environmental actions had removed some of the deposits. This study, combined with that of Sparks et al. (2002), provided the first comprehensive corroboration of the classical approach and findings of Lacroix (1904) in St Pierre.

These few pioneer studies of highly destructive PDCs were subject to various constraints presented by the eruptions and the era when the work was done. Ideally, eruption impact assessments need to be undertaken before perishable field data, such as geological deposits and building damage, are removed by rains or human activities (e.g. quarrying or clean-up). The unpredictable nature of many volcanic crises, however, means that the timing of field missions must tread a fine line between the degradation of data and the level of volcanic risk, and therefore mission safety, over time. Thus, the involvement of scientists occupied in the ongoing monitoring and emergency management of the volcano is imperative. The Merapi 2010 eruption enabled all of these challenging requirements to be met.

1.3. An interdisciplinary approach

We were able to combine remote and field assessments to investigate the volcanological characteristics of the eruption and the associated human, physical and environmental impact of PDCs in the Merapi area. These assessments represent the first unified approach to eruption impact assessment, where interdisciplinary studies were carried out contemporaneously by one field team in the same study locations and for the same key purpose: to reconstruct PDC impact dynamics and timescales and to collect important empirical damage and geological data. This combined approach allowed us to:

- Assess the main characteristics and processes of the PDCs, their hazard characteristics, e.g. minimum dynamic pressures and temperature, and the physical response of humans and their environment to such impact.
- Undertake studies that involved three different disciplines in their approach: 1) geological investigation of the deposits; 2) detailed quantitative surveys of impacted buildings, vegetation and infrastructure; and 3) medical assessment of casualty images and hospital records, and to perform these in conjunction with scientific, eyewitness and community accounts of the eruption crisis and aftermath.
- Incorporate in the overall impact assessment multiple data analysis components: remote assessment (through the use of satellite images and media footage), field assessment and associated desk-based analyses such as laboratory studies, engineering calculations and development of an extensive GIS database.

In the following sections we describe the methods and preliminary findings associated with our remote, field and desk-based studies.

2. Remote impact assessment

Remote sensing data, in the form of satellite and aerial images and also media images and footage (professional and social) freely available on the Internet, were invaluable in assessing eruption impacts. Images taken at the time of search and rescue operations were particularly valuable in showing the immediate aftermath of the PDCs. These data allowed us to monitor impacts in near real-time, identify areas where impact assessments would be most informative and map the spatial extent of deposits and damage in detail: unfeasible during field missions because of the large areas and dense populations covered. Remote sensing data, and its use within an impact assessment, can be related to three main phases: pre-eruption, syn-eruption and post-eruption.

2.1. Pre-eruption data

A fundamental aspect of eruption impact assessments is that information is available regarding the local environment prior to the eruption and its associated impacts. The ideal scenario for a well-studied volcano is that a high-resolution orthorectified image database is available; this may include satellite and aerial images as well

as images or information regarding the pre-eruption distribution and characteristics of buildings, vegetation and infrastructure (e.g. Spence et al., 2004). For the Merapi assessment, we used Quickbird (May 2006: 0.6 m resolution), Google Earth Digital Globe (September 2006: 0.5 m resolution) and SPOT5 (May 2008: 2.5 m resolution) satellite imagery to map the pre-eruption buildings and vegetation. This was particularly useful for areas completely devastated or buried by the 2010 eruption and also for identifying pre-existing damage to trees and a small number of buildings (e.g. 2006 eruption in Kaliadem) as well as pre-eruption topographic features, e.g. Sabo dams and bridges, which affected emplacement of PDCs during the eruption (Fig. 1a). In addition to pre-2010 eruption satellite images, information about how past eruptions have affected areas impacted in 2010 (e.g. Kelfoun et al., 2000; Wilson et al., 2007) was useful in identifying, for example, areas where forests may be less mature, and therefore less resistant, to impact.

2.2. Syn-eruption data

The Merapi 2010 eruption was complex and multi-stage: deposits were emplaced, and damage and casualties sustained, over different areas and with different magnitudes and intensities over a period of 11 days. Impact assessments are often not able to be carried out during an eruption because of the volcanic risk during an ongoing crisis. Long-duration eruptions like that at Soufrière Hills Volcano (1995–present) can provide an exception; however, as the study of Baxter et al. (2005) shows, syn-eruption impact assessments are often constrained by forecasting uncertainty and fluctuating volcanic activity and risk. Remote sensing data available throughout the Merapi 2010 eruption were therefore invaluable in categorising, mapping and correlating deposits, damage and casualties with time. Syn-eruption updates provided by the Indonesian Center of Volcanology and Geological Hazard Mitigation in Yogyakarta (CVGHM), the MIA-VITA project (2009–2012) and the SAFER project (2006–2009) detailed developments such as increasing evacuation zones, PDC runouts, seismicity, gas output and deformation, which were instrumental in helping us to plan and undertake field missions as soon as it was safe to do so. The 2010 eruption of Merapi provided a rare example where activity declined rapidly following the climactic eruption, allowing safe entry of field missions quickly and before degradation of deposits or damage took place. More commonly, post-eruption impact assessments may not be possible for months, or even years, after the event of interest so that syn-eruption remote sensing data or photographs may provide the only source of information from which impact assessments can be made.

Unfortunately, many syn-crisis satellite images obtained during the Merapi 2010 crisis became more easily available after, rather than during, the eruption. However, a unique feature of the Merapi 2010 eruption was that media images and footage of the damage and casualties, taken at the time of rescue, were freely available on

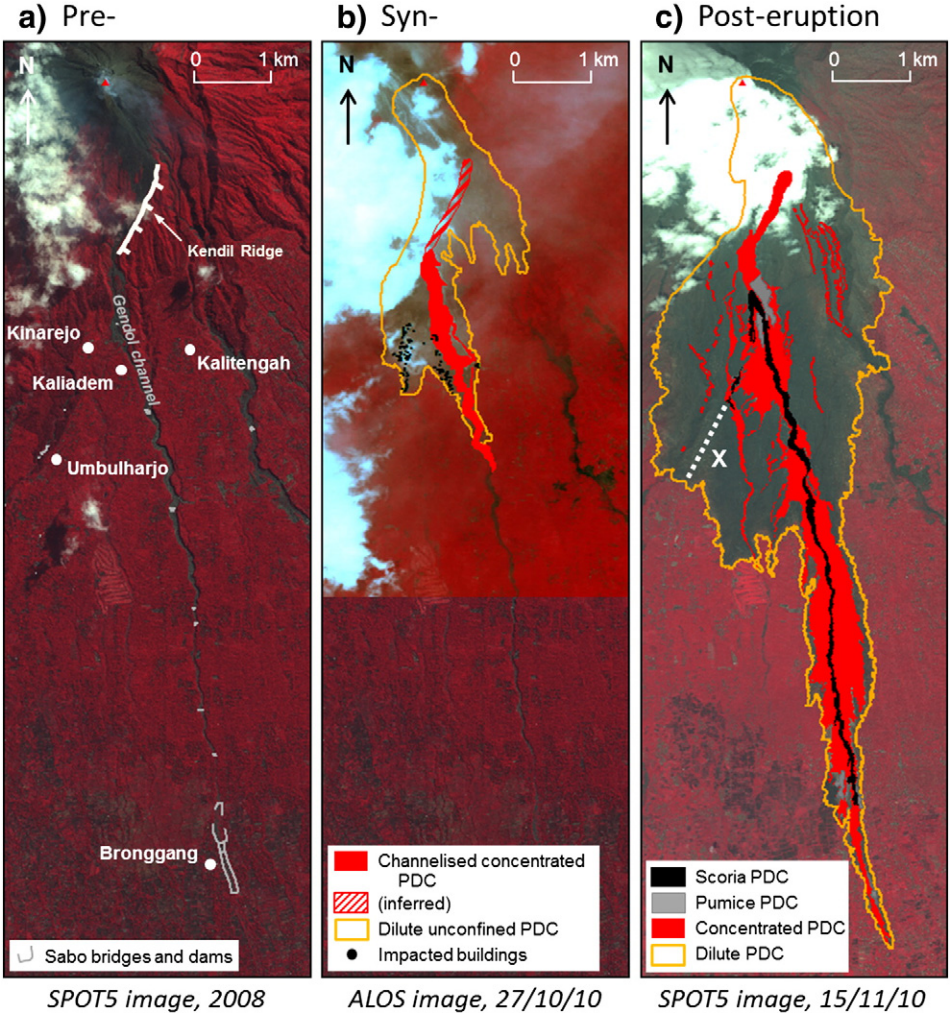

Fig. 1. a) Pre-eruption orthorectified SPOT5 satellite image (May 2008); b) syn-eruption ALOS orthorectified satellite image (29 October 2010: the lower half of the image is the pre-eruption SPOT5 image) overlain with PDC deposits associated with the 26 October PDCs; c) post-eruption SPOT5 satellite image (15 November 2010) showing the distribution of PDC deposits from the 5 November eruption, based on satellite imagery and extensive fieldwork. Building damage along transect line X in panel c is described in Section 3.2 and shown in Fig. 8. The Kendil ridge and Kinarejo, Kaliadem, Umbulharjo, Kalitengah and Bronggang villages (shown in panel a) are referred to in the text.

the Internet throughout the eruption. This is the first time graphic images of the impacts of a large explosive eruption on a densely populated area have been available uncensored and in real time, adding a new dimension to impact assessment. These images offered valuable information about volcanic activity (e.g. lava dome growth), timescales, damage, casualties and rescue operations. For example, physical evidence of damage sustained during the initial explosive event of Merapi on 26 October was subsequently destroyed by later eruptions and could not be assessed in the field (Fig. 2), beyond looking at the position of building debris within the deposits. However, by comparing damage from 26 October identified remotely (particularly in media images) with that studied in the field for areas impacted only once during the eruption we could infer approximate impact dynamics for these earlier damaging events (Fig. 2), further discussed in Section 3.2 and Table 2.

The initial 26 October event produced PDCs that spread across a 7.5 km^2 area to the south (Fig. 1b) damaging more than 150 buildings and killing 34 people, including Mbah Marijan the spiritual gatekeeper of Merapi; four people survived after hospital treatment for their burns injuries. We utilised media images, photographs and medical records provided by Dr. Sardjito Hospital (University of Gadjah Mada) in Yogyakarta and satellite images (orthorectified ALOS: 28 October and GeoEye: 29 October 2010) in mapping deposits and identifying the characteristic features of casualties and damage associated with this initial event. In particular, mapping of the deposits and images of building damage identified that the dilute unconfined PDCs of 26 October were not directly associated with channelised PDCs, being less controlled by topography and covering a wide area (Fig. 1b). This information, together with microscope observations of dominant fresh vesicular glassy fragments and fresh porphyritic andesite dome rock in the erupted deposits, elevated dome growth rates, flank deformation, high SO_2 gas output during the explosion and proximal ridge top tree orientations indicates that a laterally-directed explosion of a pressurised sealed cryptodome was responsible for these damaging dilute PDCs (see Komorowski et al., 2013 for more details).

As well as providing information on PDC impacts and dynamics during earlier stages of the eruption, media images were also useful in showing the environment at the time of impact. This was particularly informative for areas impacted during the paroxysm of 5 November, where most of our field studies were concentrated. For example Fig. 3a shows an image available online within a few hours of the 5 November event and taken during rescue operations in the village of Bronggang, approximately 13.5 km to the south of Merapi. Fifty-eight people were in the process of evacuating from the village when dilute PDCs detached from their parent channelised concentrated PDCs in the adjacent Gendol river and entered the village, killing 53 and injuring 5. From the media image shown in Fig. 3a, we could establish that casualties suffered severe burns and were coated in a layer of fine ash, as was everything impacted within the village, and that at the time of rescue (approximately 02:30, around 2 h after impact), fires were still burning and the deposits were still hot: shown by the rescuer walking on the kerb to avoid thicker deposits on the road. Media images were also useful in supporting geological evidence and eyewitness reports, for example of rainfall shortly after the 5 November climactic eruption (Fig. 3a). Finally, media images taken shortly after impact allowed us to ensure that the damage environment studied during field missions (Fig. 3b) was pristine. Preliminary results from our field studies in Bronggang village are discussed in Section 3 and in Fig. 9.

2.3. Post-eruption data

The short duration of the eruption played a large role in enabling remote damage assessment: rapid escalation towards a paroxysm that impacted an area much larger than preceding or subsequent stages and a rapid decline to eruption end meant that, for the most part, post-eruption satellite images reflect damage associated with the single climactic eruption of 5 November (Fig. 1c). High-resolution satellite imagery acquired on 10 November (Digital Globe: 0.5 m resolution) and 15 November (SPOT5: 2.5 m resolution) provided a good understanding of the deposits and impact associated with the climactic stage on 5 November 2010. For example, satellite images of the impacted area were used alongside data from our field studies to map the effects of topography on PDC behaviour, through documenting felled tree orientation, PDC overspill lobes and local variations in building damage.

By comparing the pre-, syn- and post-eruption satellite and media images we were able to map the approximate building damage remotely (Fig. 4). The majority (n = 1411) of affected buildings (n = 2268) were damaged by high- and low-energy dilute PDCs (surges) and not by concentrated PDCs (flows). In areas affected by concentrated PDCs (7 km^2), building devastation was complete with most buildings and

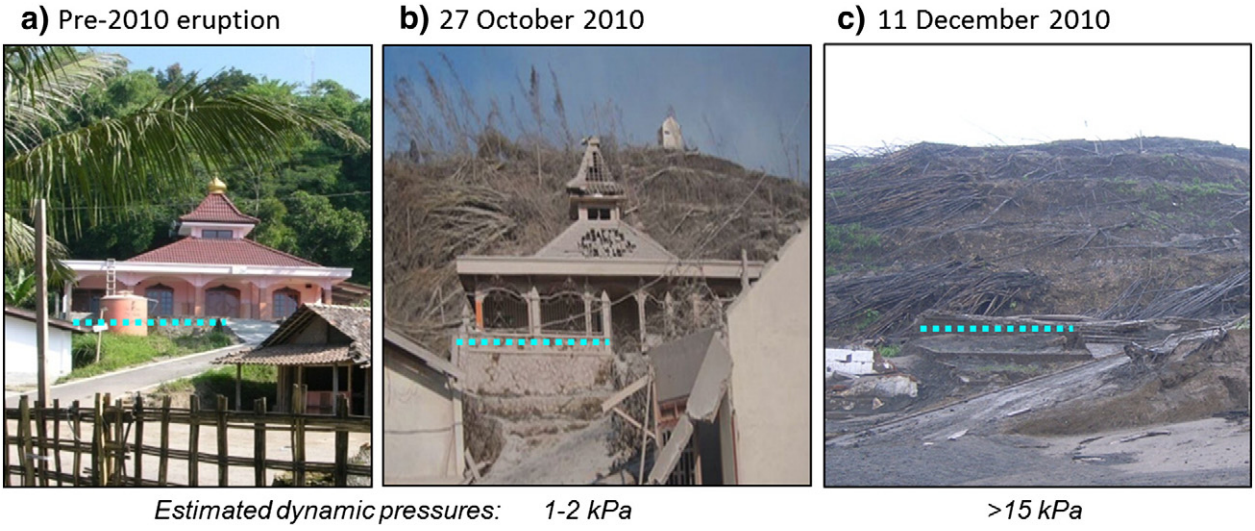

Fig. 2. Photographs of the Al Amin mosque in Kinarejo taken a) In 2008 prior to the 2010 eruption; b) As rescue teams entered the impact area on 27 October, one day after the first eruption (images from merapi.info); and c) during our field mission in December 2010 (image: S.Jenkins). The hashed line shows the mosque foundations in the three images and approximate dynamic pressures have been estimated from field studies of the area and building typologies and theoretical calculation of their structural resistance (see Section 3.2 and Table 2 for further details).

Table 2
Measured parameters, dynamic pressure calculations and assumptions from assessing the level of damage to buildings (n = 89), trees (n = 26) and the transport of missiles (n = 42) across the proximal impact area. Other measured impacts that provided information on dynamic pressures (n = 37) include impact marks, damage to openings, the lifting and transport of roof tiles and the failure of freestanding objects such as concrete electricity poles and gateposts. A vertically uniform current is assumed for all calculation methods and SI units are used.

Object:	Buildings	Trees	Missiles
Impact	Wall failure	Felled	Deposited from the PDC
Value	Minimum (damage) or maximum (no damage)	Minimum (felled) or maximum (not felled)	Maximum
Parameters measured	–Level of damage (e.g. zero, partial or total); –Orientation and sheltering; –Dimensions of structure (e.g. wall) and its components (e.g. bricks); –Size, location and type of openings; –Reinforced concrete bar locations and dimensions within columns and beams	–Level of damage (e.g. upright, snapped, felled); –Orientation and sheltering; –Dimensions (height, circumference); –Extent of delimbing; –Tree type	–Dimensions; –Shape (e.g. compact, rod, sheet); –Material (later laboratory analysis of samples allowed us to establish density); –Distance carried (where possible)
P is the dynamic pressure required to	Cause wall failure	Fell trees	Keep missiles in flight
Calculation	$P = [(2\mu + 2\beta^2/\alpha^2)/(3\beta - 2\beta^2)].\ f_n.\ (t/w)^2$ Where: μ Is the ratio of the vertical to horizontal modulus of rupture (2 for buildings at Merapi) β, a constant ($0 < \beta < 0.5$) giving the location of the point where the fracture line meets the free top edge of the wall. β is varied to minimise the lateral pressure α is the ratio of the wall height to its width (w) f_n is the modulus of rupture of the brickwork about the horizontal bed joint (0.15 to 0.45 N/mm^2) t,w are the wall thickness and width	$P = M_{u,y}/r.\ h^2.\ C_D$ Where: $M_{u,y}$ is the bending moment at failure (M_u) and the moment at yield (M_y) given as $1.36 \times 10^7.\ r^3$ r is the trunk radius h is the tree height C_D is the coefficient of drag (1.1 for a delimbed tree)	$P = d.\rho_m.g/C_f$ Where: d is the missile diameter ρ_m is the density of the missile material g is acceleration due to gravity C_f is the force coefficient (1 for compact objects)
Reference	Following Hendry et al. (1997)	Clarke and Voight (2000)	Wills et al. (2002) and Spence et al. (2007)
Assumptions	Failure follows fracture lines; Wall supported on three sides[a]; No openings.[b]	Failure at the base; Vertically uniform trunk; No branches or canopy remain.[c]	Compact object[d]; Objects are loose prior to transport.

[a] Pre-compression load on the top of a wall from heavy roof materials increases failure load but is not applicable for the majority of structures at Merapi.
[b] It is not clear whether openings strengthen or weaken a panel. Field observations on Merapi suggest they may strengthen the panel because of the strengthening effect of the window frame, lintel and cill, and so failure pressures calculated likely represent conservative minimum estimates.
[c] Many of the trees in the Merapi area were delimbed from increasing dynamic pressures, for trees that retained some branches and therefore failed at lower dynamic pressures because of the increased frontal area we followed the method of Clarke and Voight (2000) in calculating dynamic pressures.
[d] The majority of missiles were compact objects, for calculating dynamic pressures from transport of sheet and rod missiles we followed the method of Wills et al. (2002) and Spence et al. (2007).

infrastructure buried except for those on the very peripheries. In proximal (<9 km) areas affected by the high-energy turbulent stratified PDCs, there was a sharp attenuation in building damage, and therefore in lateral dynamic pressures, within approximately 1 km of the runout limit reducing from completely destroyed buildings, where no footprint remained, to removal of the roof structure, to buildings where the structural fabric remained intact (Fig. 4d). Casualty images provided by the media and Dr. Sardjito Hospital, along with our field investigations, confirmed the high lethality of even low-energy dilute PDCs that detached from parent channelised concentrated PDCs at their farthest extent, more than 15 km from the volcano. Taking a conservative estimate of 5 persons per household, we can therefore approximate that more than 11,000 lives were saved by evacuations, in line with other estimates (Surono et al., 2012). While invaluable in mapping damage across large areas, remote assessment of building damage does not show the resistance of different building types to dynamic PDC impacts such as pressure, temperature or missiles. In some areas on Merapi (Figs. 1 and 2), buildings were impacted multiple times (e.g. Kinarejo) and repeated impacts may have weakened the structure prior to the 5 November event — this could only be confirmed through field studies. Our field studies therefore greatly improved our understanding of the nature and severity of building damage by allowing us to reconstruct the PDC impact dynamics.

3. Field impact assessment

At the invitation of the Indonesian Center of Volcanology and Geological Hazard Mitigation in Yogyakarta (CVGHM), and under the umbrella of the MIA-VITA (2009–2012) and CASAVA (2010–2013) projects, we undertook three field missions in areas impacted by the 2010 eruption at three weeks, eight months and one year after the eruption. Impact data were collected across the three missions because of the extensive time requirements associated with their collection, the necessity for analyses of deposits prior to and after rain erosion and to refine our assessment methodologies over time with the collection of additional data. One purpose of the field missions was to calibrate our findings from the remote assessment (building damage and deposits) and to carry out extensive and interrelated studies of the pristine deposits, damage and casualties. A further benefit of field studies was that we were able to verify the eruption chronology in terms of monitoring data, crisis management and population movement, i.e. evacuation orders and compliance. The relatively quick decline in eruption activity allowed field teams to safely enter impacted areas within one week of eruption end on 23 November. The studies focussed together on areas of greatest impact and assessed the impact of PDCs associated with five different processes: dome explosion, dome collapse, column collapse, PDC overspill and PDC detachment. Three interdisciplinary field studies were conducted in parallel, as described in the following sections.

3.1. Geological studies

Geological studies were co-ordinated with damage and casualty studies to allow accurate reconstruction of events in areas of significant damage or deaths, but also undertaken in areas that are important for understanding the PDC dynamics, e.g. proximal unpopulated locations and in the Gendol channel. Fieldwork was carried out at 109 detailed field sites (291 study sites in total) within the impacted area between

Fig. 3. Photographs of Bronggang village, approximately 13.5 km from Merapi volcano and impacted by dilute PDCs that detached from channelised PDCs in the Gendol river channel (back right of images) on 5 November. Photographs were taken: a) At approximately 02:30 on 5 November 2010 during rescue operations (Boston.com, 2010); b) On 6 December 2010 during our field studies (S. Jenkins). Media images were used to infer the severity of casualties and damage at the time of impact and to ensure that the impact environment was pristine at the time of our field mission.

2.5 and 15.5 km from the crater, and 223 samples of erupted material were collected for laboratory analysis. We have reconstructed the timescale, source processes and transport and depositional characteristics of the diversity of PDC deposits through a combination of detailed stratigraphic and field analysis, sedimentology and microscope observations of pyroclastic material (geological analyses of the 5 November proximal PDCs are presented in Komorowski et al., 2013; future publications will detail other stages of the eruption).

Our studies show that five main types of primary PDCs were produced within the first 30 min of the 5 November climactic eruption (Table 1) and are characterised by marked differences in distribution, dynamic characteristics and impact. They are: 1) unconfined high-energy turbulent stratified PDCs from dome explosions; 2) channelised high-energy block-rich PDCs from dome explosions; 3) channelised concentrated block-rich PDCs from dome collapse; 4) overbank PDC lobes from the channelised concentrated block-rich PDCs; and 5) dilute PDCs that detached from the main channelised block-rich PDCs (the most important, in terms of mortality, being at Bronggang village). Despite their contrasting origin and lithofacies characteristics, type 1 and 5 would fall in the overall category of pyroclastic surges while types 2, 3, and 4 would fall in the category of pyroclastic flows. This resulted in a very complex stratigraphy for the primary depositional units, particularly for the proximal high-energy PDCs, which were strongly affected by topography and characterised by significant lithofacies variability with distance from the main PDC axes and from the crater. Reconstruction of the nature, timing and extent of processes and associated deposits from the initial dome explosion PDCs of 5 November is further complicated by the contemporaneous emplacement of at least two unconfined high-energy stratified PDC units that we correlate with distinct pulses initiated by explosions at 00:06 and 00:09 local time (UTC + 7 h) and with their channelised contemporaneous counterpart PDCs (block-poor and block-rich facies). These PDCs could be distinguished from earlier less energetic dome explosion PDCs emplaced between 26 October and 4 November by their distinctive bipartite deposits (i.e. a lower very coarse-grained, fines-poor, poorly-sorted and massive unit overlain by a much finer grained, fines-rich, moderately to well-sorted unit with laminar to wavy stratification), strongly directional tree blow-down and widespread devastating impact, which shows marked similarities with well-studied historical blast PDC deposits (e.g. Belousov et al., 2007). We propose that localised increases in PDC impact dynamics at distance from source on 5 November were caused by the influence of a horseshoe-shaped crater and strongly constrictive topography along the PDC path, in concert with kinetic energy gained from the significant elevation drop (>2000 m from summit to settlements), and travel over recent smooth PDC deposits, to produce PDCs analogous to a volcanic blast (for further details see Komorowski et al., 2013). Quantitative data collected as part of this study may provide valuable information to support modelling of such effects (e.g. Esposti Ongaro et al., 2008, 2012).

In addition to providing a process-orientated interpretation of the PDC deposits, geological field studies delivered key information on PDC dynamics, e.g. velocity (Komorowski et al., 2013), independently from those derived from damage so that estimates could be cross-correlated and calibrated. Through our field missions, we have thus been able to verify mapping of deposits from remote satellite imagery (Fig. 1c) and also to identify distinctive PDC units such as the bipartite blast-like deposits of 5 November and key chronostratigraphic layers such as accretionary lapilli ashfall units, which provide indication of a hiatus in PDC emplacement and presence of a primary surface (Fig. 5). Geological field studies also enabled us to record the timing and characteristics of recurrent impacts throughout the eruption; for example, remote sensing data showed that Kinarejo village, approximately 4.5 km from the volcano, was impacted more than once (Fig. 1) but through field studies we could establish that the area was actually struck by seven distinct PDCs between 26 October and 4 November, before being covered by a further 66 cm of deposit on 5 November (Fig. 5). To support, or in the absence of, syn-crisis satellite or media imagery in such areas with recurrent impacts, the timing and extent of building damage could be established from their position within the deposits.

3.2. Damage to buildings, infrastructure and vegetation

Our damage studies concentrated mostly on 1) proximal (<9 km) impacts associated with the 5 November high-energy PDCs, which caused devastation to structures and forest across a wide evacuated area on the southern flanks (22 km^2); and 2) distal (9–16 km) impacts where dilute detached and concentrated overspill PDCs entered villages adjacent to the Gendol channel killing a large number of people (>120) as they were in the process of evacuating (Fig. 3). For the Merapi area, a good understanding of the pre-eruption building vulnerability with respect to lateral loading (one of the principal damaging mechanisms associated with earthquakes and high-energy PDCs) was obtained from reviewing building damage studies carried out following the May 2006 Java earthquake (EERI, 2006). However, other important lessons regarding building vulnerability, such as the extent and positioning of ventilation that permitted infiltration of dilute PDCs, were only established through field studies.

We performed detailed quantitative ground surveys of more than 150 impacted buildings, as well as damaged vegetation and infrastructure,

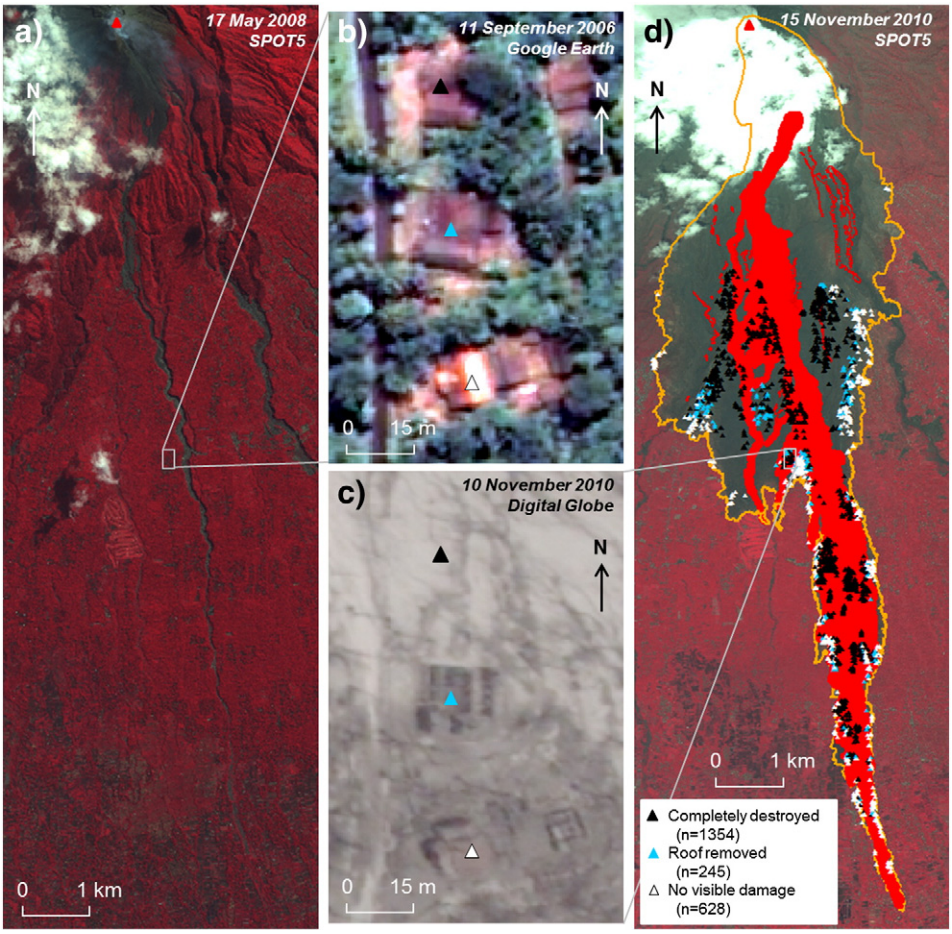

Fig. 4. a) Pre-eruption SPOT5 satellite image, which was used with other pre-eruption information and satellite images to map pre-eruption building locations; b) pre-eruption satellite images of the 2010 eruption impact area could then be compared with c) post-eruption satellite images to plot building damage remotely; d) the level of damage sustained by buildings from the 5 November PDCs. With a conservative estimate of 5 people per household, we can approximate that more than 11,000 lives were saved by evacuation measures.

across the proximal and distal impact areas, in which we documented the building dimensions, construction materials and the level and type of damage (Table 2). These data were subsequently recorded in a GIS database so that we could correlate remote and ground-sourced data and investigate the damage with distance from the crater and PDC axes and relate damage with deposit facies and topography. Further quantitative estimates of the impact dynamics were obtained regarding the frequency, severity and size of missiles (e.g. building debris, dome rock) and missile impacts, the orientation of damaged components, and therefore the current direction. The height of pockmarks on tall objects such as electricity poles and trees acted as a proxy for the minimum height of the high particle concentration part of the stratified PDC.

3.2.1. Dynamic pressures

Using these data and theoretical calculations of material and structural resistance to lateral dynamic pressures (see Table 2 and Fig. 6 for methods), we could derive approximate dynamic pressure values ($n = 164$), and therefore contours, across the proximal impact area (Figs. 6 and 7). In peripheral areas of minimal damage, dynamic pressures of less than 1 kPa could be derived from calculating the failure pressures of downed concrete electricity poles and trees (Table 2 and Fig. 6, following Clarke and Voight, 2000) and the lifting of roof tiles and lightweight sheeting (following BSI, 1997). In areas of heavy or moderate damage, the range of dynamic pressures was best estimated from buildings, trees and structures that did (minimum pressure estimate) or did not (maximum pressure estimate) fail. The effect of wall thickness and span on building vulnerability to PDCs was evident across the impact area at Merapi, with thick (25 cm) rubble stone masonry and short-span walls offering more resistance than thinner (10 cm) concrete block masonry and long-span walls, even those strengthened with a reinforced concrete frame (Fig. 6). Therefore, at any one site multiple dynamic pressure estimates could be made from field measurements and observations. For example, field measurements for a partially collapsed building (Fig. 6b) can provide maximum dynamic pressure estimates from the parts of the building that did not fail (i.e. had the dynamic pressure exceeded this value failure would have occurred) and minimum dynamic pressure estimates from the components that did fail (e.g. because of a longer-span wall or less resistant building material). Transport, or otherwise, of the building debris of different sizes downslope from the structure and damage to nearby trees and manmade structures such as gateposts, signs and water tanks, could also provide minimum and maximum dynamic pressure estimates. The main limitation we found in calculating approximate dynamic pressures from building damage on Merapi is the lack of available knowledge about the strength of building components, e.g. mortar, because of the varying levels of construction and material quality and the age and condition of a building. We have accounted for this in our estimates by identifying lower and upper bounds for each parameter from strength tests, literature and expert judgement and thus calculating conservative minimum and maximum dynamic pressures (Fig. 6). In this way, one site may have a range of dynamic pressure estimates, which when considered in combination with field and satellite images of the site, and with potentially influential factors such as sheltering, could be used to manually interpolate approximate dynamic pressure values for that site and contours across the impact area (Figs. 6 and 7).

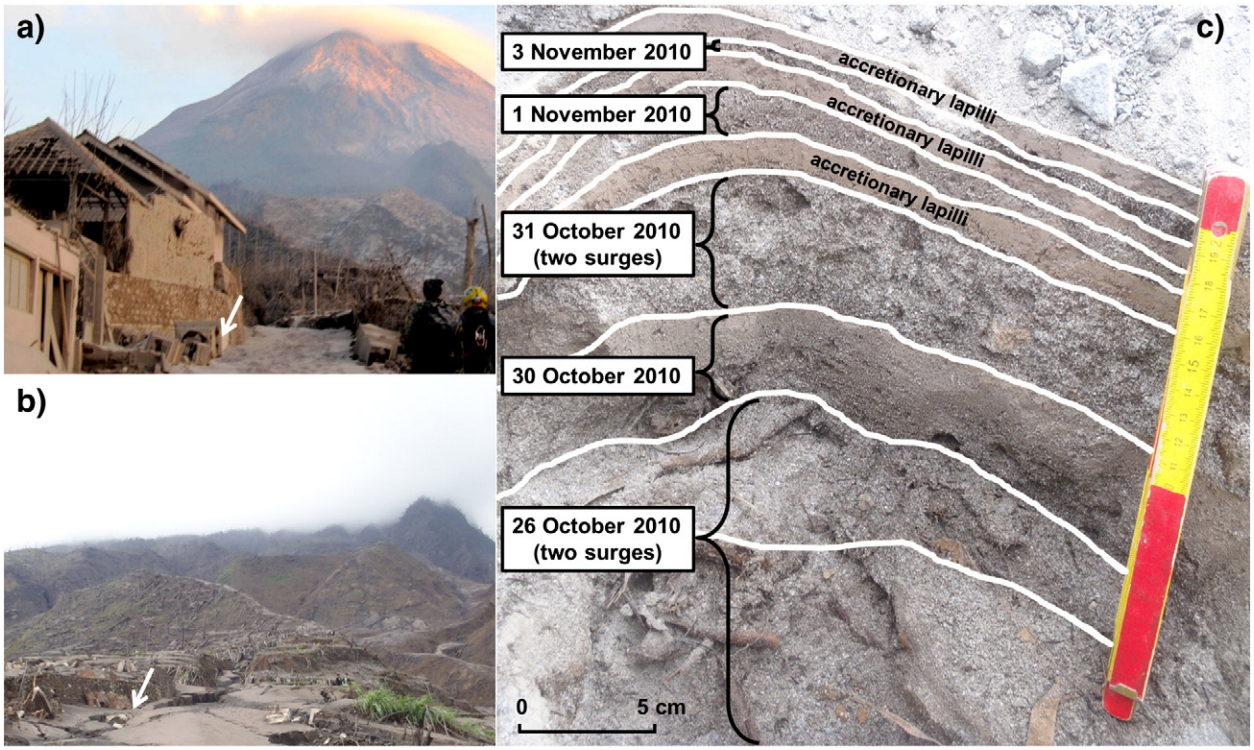

Fig. 5. Photographs show a) 27 October media image of Upper Kinarejo taken as rescue teams searched for survivors (Eko Susilo Blogspot, 2011); b) the same location on 11 December 2010 during our field mission (J.-C. Komorowski); and c) annotated stratigraphy shows the passage of seven dilute PDCs between 26 October and 4 November at the location marked by arrows in photographs 5a and b. The climactic 5 November eruption emplaced a further 66 cm deposit on top of the stratigraphic section shown in 5c. The location of Kinarejo is shown in Fig. 1a.

These estimates, and the perceived relationship between dynamic pressure and damage level for impacted objects, could then be used to approximate dynamic pressures for similar damage observed in media images (e.g. 26 October in Kinarejo: Fig. 2) but for which field observations were not possible because of subsequent activity. For example, the felling of slim trees and bamboo in Kinarejo on 26 October (Fig. 2) suggests dynamic pressures of 1 to 2 kPa (Clarke and Voight and Table 2), which is supported by a lack of significant structural damage to the weak reinforced concrete frame masonry buildings, which fail at pressures of around 2 to 4 kPa (Table 2, Spence et al., 2004). Subsequent high-energy PDCs on 5 November completely destroyed all previously damaged buildings in this area, with building debris removed from the area by the PDC. In areas of complete destruction, identifying an upper limit to dynamic pressures was typically reliant upon a small number of robust structures and upon calculating pressures required to keep missiles transported in the PDC (following Wills et al., 2002; Spence et al., 2007: Table 2), where missiles generally comprised dome rock or building debris (Fig. 6). The transport of large (>1 m diameter) missiles and damage to robust structures suggests dynamic pressures in excess of 15 kPa up to 6 km from source (Fig. 7) however our findings showed that the vast majority of structures were destroyed by dynamic pressures lower than 5 kPa because of poor quality construction and low mortar and brick strength. Dynamic pressures in excess of 5 kPa are required to lift building debris larger than 30 cm across (following Spence et al., 2007) and so the majority of buildings were destroyed at dynamic pressures lower than those where we would expect to see damage from missiles in flight, e.g. puncture holes in walls.

Local variability in the PDC dynamics, interaction with topography and different building construction styles, materials and standards, tree size and strength, resulted in significant variability in damage within a small area (tens of metres); however, damage was clearly gradational with distance from the volcano and from the main channelised PDC axes, rapidly attenuating towards the peripheries of the high-energy dilute PDCs (Figs. 6 and 7). Axes of increased damage and missile transport, and therefore larger dynamic pressures, are clearly correlated with the Gendol and Opak channels. This suggests interaction of the PDCs with topography leading to increased dynamic pressures in valleys where the current was more dense, which is supported by geological studies (see Komorowski et al., 2013). Damage at Merapi was total to within 1 km of the PDC runouts (Fig. 8), indicating the remarkable attenuation in dynamic pressures as the PDC came to a halt on the flank. At the same time, the gradient reveals the low resistance of Merapi buildings to lateral dynamic pressures associated with the high-energy PDCs. The orientation of a building can influence at what dynamic pressure failure takes place, however buildings on the slopes of Merapi are built on terraces with the front of the building facing downslope and the rear facing the volcano. All walls used in our calculations were orientated approximately perpendicular to the current direction so that building orientation was not a factor in calculating failure pressure. Few impact studies of destructive high-energy PDCs have been conducted previously and the Merapi eruption provides a first evaluation of the damaging nature of small-scale high-energy PDCs (affecting <50 km^2) to the end of their runout: comparable high-energy PDCs at Mt Pelée on 8 May 1902 and Soufrière Hills Volcano on 26 December 1997 were still highly damaging when they entered the sea up to 5 km from the vent.

3.2.2. Temperatures

Unlike the high-energy PDCs of Soufrière Hills Volcano and Mt Pelée, where temperatures of 300–400 °C (Tanguy, 1994; Sparks et al., 2002) resulted in combustion of furnishings and other flammable objects from the heat of the deposits, fires were not widespread at Merapi, suggesting temperatures lower than 300 °C. Indicators of thermal damage alone were remarkably few, but included melting plastic pots (>170 °C: Voight and Davis, 2000), singed acrylic and

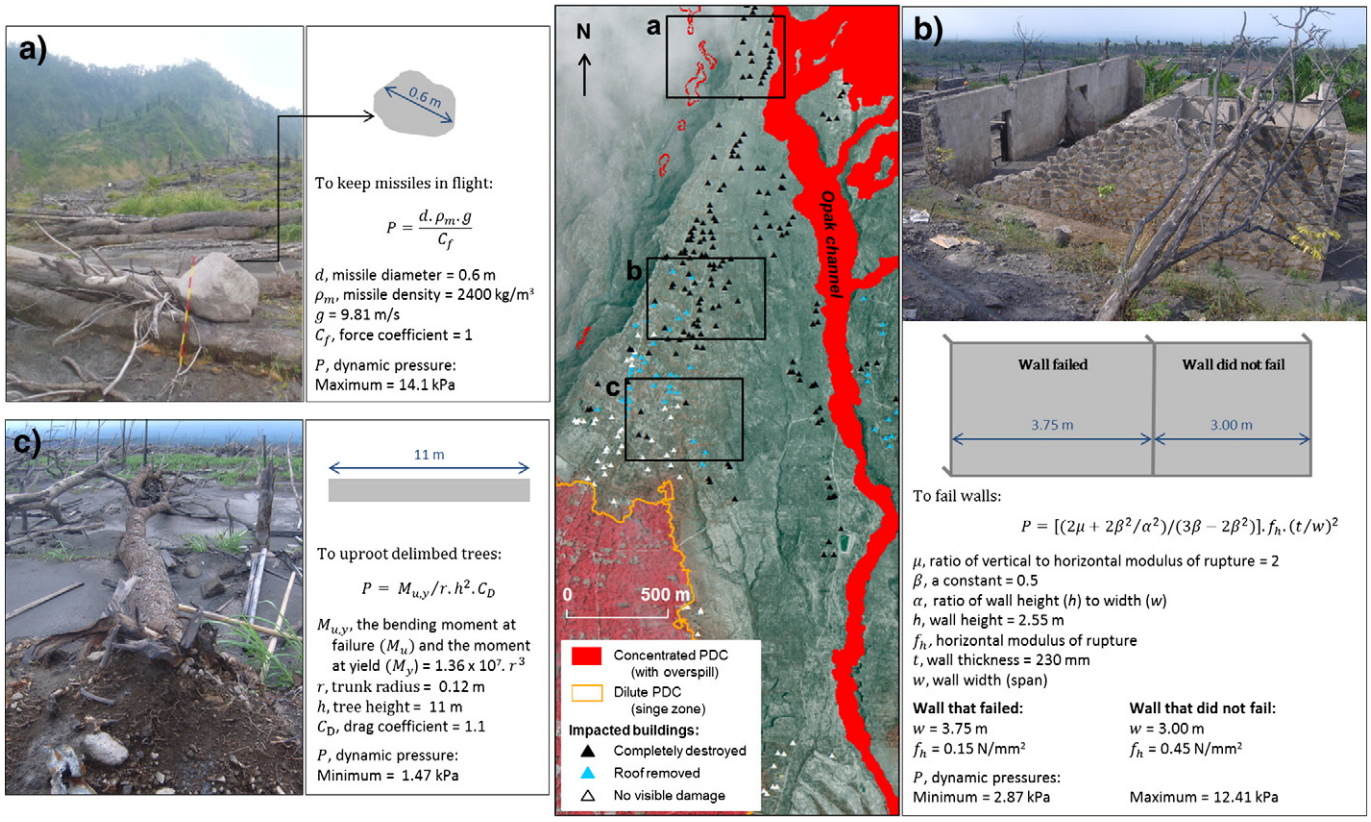

Fig. 6. Dynamic pressure calculations for selected damage in Kinarejo and Umbulharjo (approximately along transect line X, Fig. 1). Estimates of dynamic pressure at any one location are constrained from multiple dynamic pressure indicators and, in concert with satellite and field images and consideration of potentially important effects such as sheltering, are used to infer dynamic pressure contours across the impact area (Fig. 7). The main source of uncertainty in estimating wall failure pressures is the modulus of rupture of the brickwork about the horizontal bed joint (f_h). We consider a credible range (0.15 to 0.45 N/mm^2) based upon damage studies following the 2006 Java earthquake and expert judgement and sample from the lowest value for walls that failed (to give a conservative minimum failure pressure) and the highest value for walls that do not fail (maximum pressure resisted). Dynamic pressures are converted from Pa to kPa. Further information on the methods used are provided in Table 2 and Section 3.2.

nylon clothing (<400 °C: TNO, 1992) and papers or books (char temperature dependent upon thickness). The proximal high-energy PDCs at Merapi were characterised by approximately similar temperatures (200–300 °C) to the much smaller 22 November 1994 dilute PDC at Merapi (Voight and Davis, 2000) but were lower than those experienced at Mt Pelée (~400 °C) or Soufrière Hills Volcano (~300 °C). We propose that the relatively low temperatures at Merapi resulted from 1) chiefly the comparatively much smaller magma volume (5 million m^3 dense-rock equivalent: Surono et al., 2012) involved in the explosion than at Mount Pelée (~20 million m^3: Tanguy, 1994) and Soufrière Hills (~40 million m^3: Sparks et al., 2002); coupled with 2) the effects of major constrictive topography initiating lift off and associated entrainment of cooler ambient air; 3) the incorporation of large volumes of water-saturated rock in retrogressive collapse of the dome and upper edifice that hosted the hydrothermal system, as evidenced by a widespread accretionary lapilli ashfall unit comprising hydrothermally altered material emplaced shortly after eruption onset on 5 November; and 4) possibly an interaction of PDCs with dense tropical vegetation on the upper slopes, which may have acted as a heat sink.

Topographic path effects upon the 5 November PDCs, along with infilling of the upper Gendol valley by PDC deposits emplaced prior to 5 November (to 12 km) aided the long runout of the channelised PDC components into the Gendol channel, to a radial distance of more than 15 km (17.6 km flow distance). Channel morphology and lahar mitigation structures (Sabo dams and bridges) acted to initiate PDC detachment and overspill into inhabited areas. We focussed our distal (9–16 km) studies in Bronggang (Fig. 1a), 13.5 km from the volcano and where 58 people were caught by a slow-moving dilute detached PDC before they could evacuate. Despite the lethality of the dilute PDCs (53 killed outright or fatally injured), damage to buildings, infrastructure and vegetation was minimal with bending of bamboo and lifting of a small number of roof tiles, which occurs at dynamic pressures of less than 1 kPa. Serious damage (six buildings destroyed) in the village resulted from isolated fires. A good understanding of the local customs was important in understanding the damage sustained: for example, timber frame lean-tos generally housed an outdoor kitchen where highly flammable or fire-potentiating items like kindling wood, firewood and gas cooking canisters would be kept. Our field studies in Bronggang found that in all cases these lean-tos ignited and in some the fires spread into the adjoining masonry homes and were potentially intensified by butane/propane gas release from stove gas cylinders. In at least one building, we found a motorbike where the petrol tank had been ruptured by the heat allowing the release of a stream of petrol vapour. Motorbikes were routinely kept inside homes overnight and were the main mode of transport in the evacuations. The spread of fire from the lean-tos would have threatened any injured occupants and escape from the fires would have been impeded by the high temperature of the ash deposits outside the houses. We inferred that the isolated fires were triggered by firebrands transported in the dilute PDC when it detached from the main channelised PDC in the Gendol channel and not by the hot deposits, as these infiltrated all buildings but did not cause widespread fires.

3.3. Casualties and eyewitness accounts

Information regarding burns casualties (deaths and injuries) from the 2010 eruption was collected by PJB (a medical doctor) in collaboration with doctors and surgeons at Dr. Sardjito Hospital in Yogyakarta, which was the main hospital for receiving victims during the eruption.

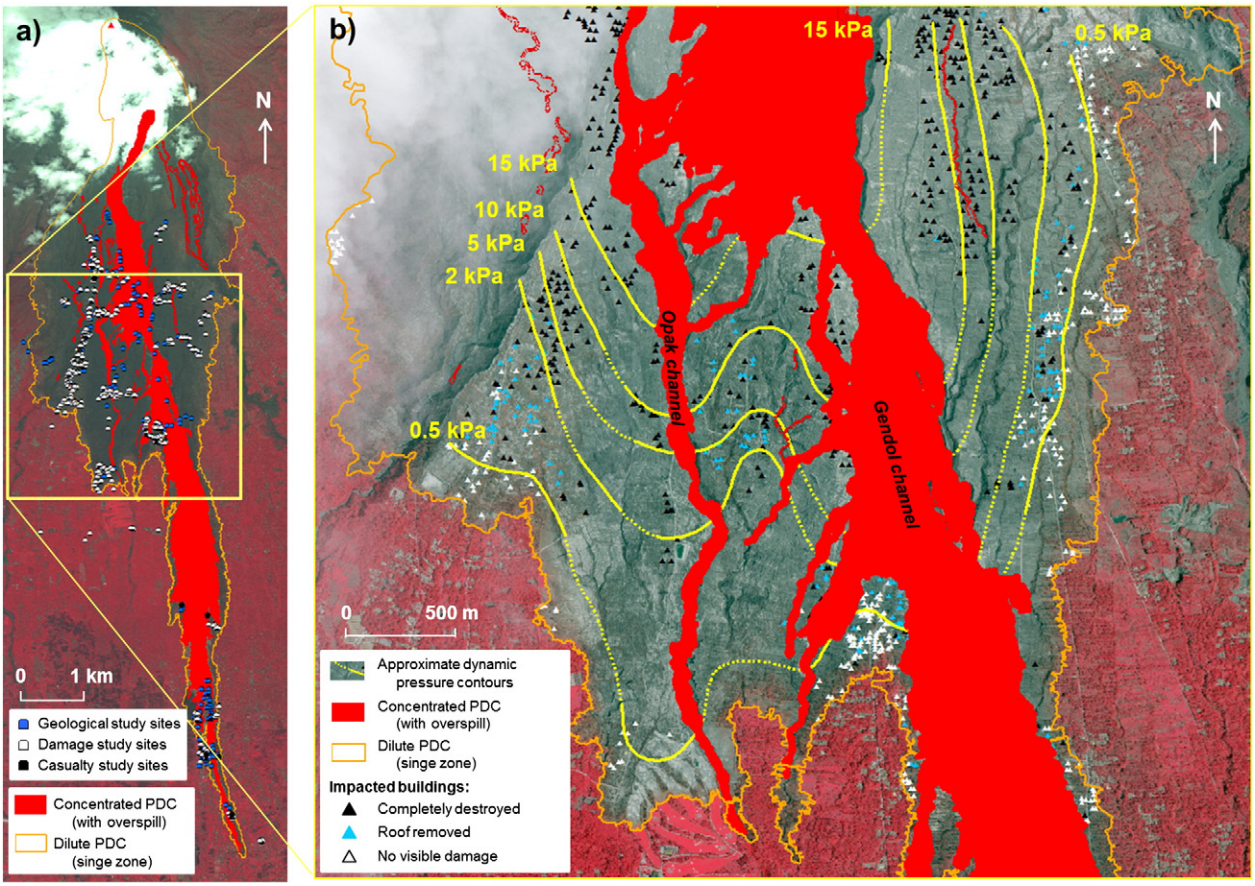

Fig. 7. a) Field study sites across the impact area with inset box, b) approximate dynamic pressure contours in the high-energy PDC impact area, derived from extensive field damage studies and theoretical calculations of structural and material resistance to dynamic pressures. Dashed contours indicate where estimates are subject to larger uncertainties because of a lack of damage data. Digital Globe satellite image taken 10 November 2010 at 0.5 km resolution.

Admittance, treatment and mortuary records and photographs were also utilised. As is the religious custom, autopsies were not carried out, but the victims were examined for identification and death certification purposes. The areas of highest human impact were villages bordering the Gendol river more than 12 km from the volcano, where people heard about or responded to the evacuation orders only shortly (hours to minutes) before the PDC arrived, and where residents may have been less prepared for or aware of the danger given the relatively large distance from the volcano and the perceived protection that was given by 6 to 7 m high Sabo walls along the river banks.

A rich source of casualty and crisis management information came from interviews with survivors of the PDCs and with village chiefs. We employed a fluent Javanese interpreter for the interviews to limit the effects of mistranslation and to aid understanding of the local cultural beliefs and characteristics, for example the way in which experiences are recounted (temporal and spatial reference) and the incorporation of rumours and hypotheses. Eyewitness and village chief accounts were correlated with interpretation of the eruption timing and chronology from seismic records (Budi-Santoso et al., 2013; Jousset et al., 2013) and with the geology (Komorowski et al., 2013) to show that PDCs reached the villages approximately 15 to 30 min after the climactic dome explosion and collapse stage began around midnight on 5 November (local time: UTC + 7 h). From media and mortuary images of the casualties sustained during the 26 October and 5 November PDCs, and from survivor accounts, we could deduce that fatalities were rapid onset and accompanied by severe skin or inhalation thermal injury sustained from dilute detached PDCs and direct burning from contact with concentrated PDC overspills. Some corpses showed evidence of being caught in fires, while others were suggestive of death from the heat of the PDCs only, with all victims covered in a thin layer of fine, adherent ash. However, the ground deposit of ash remained very hot for hours after the event (Fig. 3a) and walking in the ash without adequate protection did, in some patients, cause severe burns to the feet. Media images and footage were invaluable in helping us to identify the location of certain casualties, with respect to their impact environment and the PDCs as well as the severity of their injuries (Fig. 3a).

As in proximal areas, the temperatures associated with PDCs were derived from cataloguing the thermal effects on building components and contents such as timber, clothing and thin plastics and these observations were analysed in concert with satellite imagery and field mapping of the heat effects on vegetation to establish crude isothermal contours for the dilute PDC cloud. In Bronggang we were also able to study the effects of the heat on humans from photographs of cadavers recorded by the Dr. Sardjito Hospital mortuary. Using the still incomplete hospital records available to us we identified five intact bodies reported to be found in Bronggang that were fixed in a pugilistic attitude (limbs flexed and spine extended: Baxter, 1990) with no evidence of having been caught in a fire. The eyewitness account of one survivor who escaped shortly after the dilute PDC entered the village observed that one of these victims was lying on the ground in this state after the PDC had lifted. The pugilistic attitude denotes a temperature of at least 200 °C around the time of death for burns to penetrate below the skin layer and involve the limb muscles leading to their fixed contraction (Baxter, 1990). We consider that the dilute PDC temperature in Bronggang was in the range of 200–300 °C to lead to this attitude in death, with a peak duration of 2 to 3 min. Despite the low structural damage and low velocity of the dilute PDC,

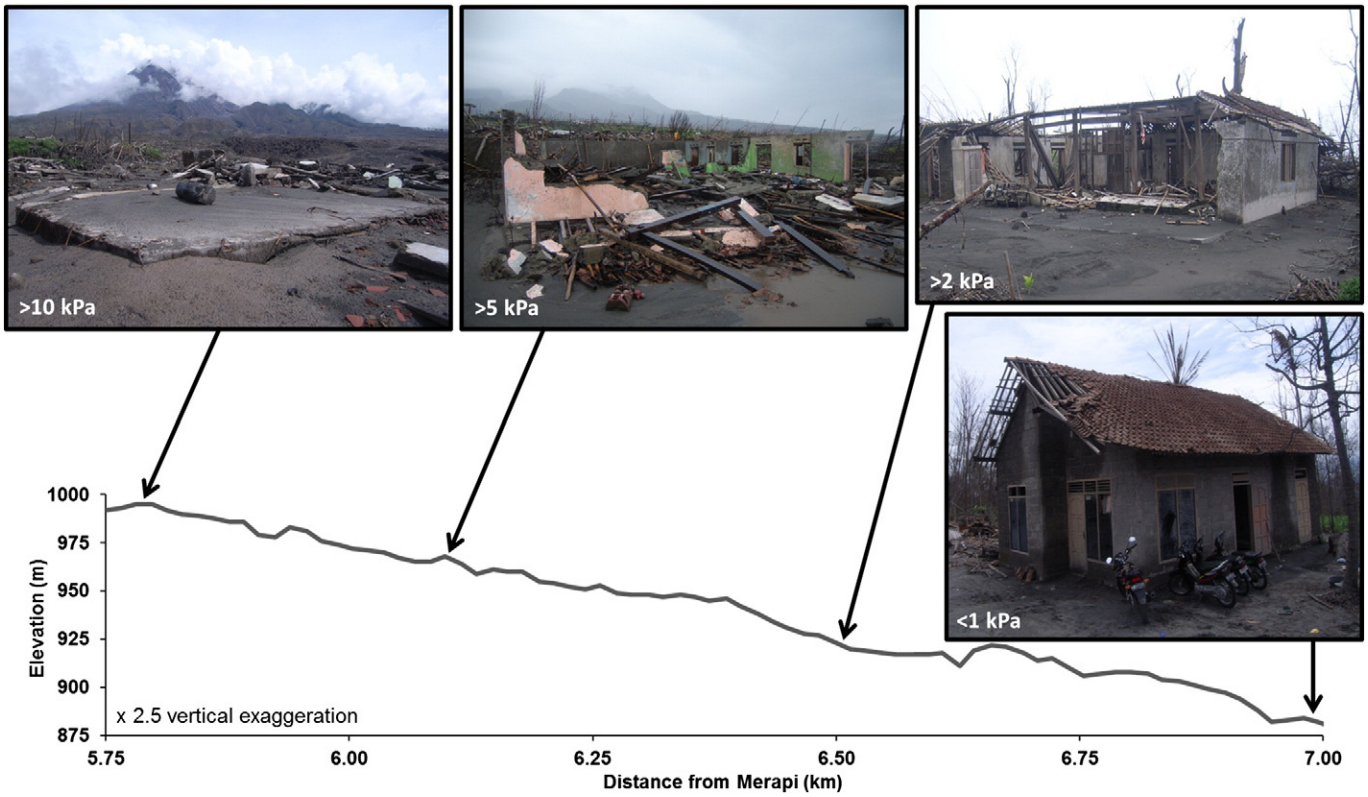

Fig. 8. Building damage and calculated dynamic pressure values along transect line X west of the Opak channel (shown in Fig. 1c). Damage rapidly attenuates over a distance of approximately 1.25 km at the periphery of the 5 November high-energy PDC. Photographs: S.Jenkins.

temperatures of 200–300 °C were deadly in residents caught outside and inside buildings as in the latter case the dilute PDC could infiltrate, even when all the windows and doors were closed at night, through ventilation openings (wall grills and spaces between the top of the wall and the roof) that all homes possessed. This efficient infiltration led to deposition of 5 to 10 cm of very fine-grained ash (25 vol% less than 10 μm) in buildings enveloped by the dilute PDC cloud. It is likely that with the low dynamic pressure and short duration of the peak temperature people could have survived inside buildings if the ventilation openings had been well sealed. Most survivors who lived long enough to reach hospital required intensive burns treatment as they suffered widespread skin burns and almost invariably some degree of inhalation injury.

4. Discussion and conclusions

The Merapi 2010 eruption provided a rare and important opportunity to study the lethal and damaging impacts of highly dangerous PDCs. With favourable conditions, i.e. escalating volcanic activity, adequate monitoring and the availability of high-resolution daily radar imagery, it proved feasible to rapidly evacuate more than 400,000 people to official shelters in a scaled response during the Merapi 2010 eruption. Such a rapid evacuation and displacement of hundreds of thousands of people had not been tested before in a highly hazardous explosive eruption. A number of evacuation shelters required relocation with the expansion of exclusion zones, placing further strain upon evacuation logistics, finances and the wellbeing of evacuated people. More than 2200 buildings were damaged by PDCs, approximately 1600 beyond simple repair, with areas up to 6 km from the vent completely devastated. More than 120 people were killed in villages at least 12 km from the volcano after being caught in PDCs, many as they were in the process of evacuating. The 2010 crisis is therefore a seminal eruption in providing empirical PDC impact data and key lessons for future volcanic crises in densely populated areas or where there are few available options for evacuations or relocation, e.g. small islands.

We carried out quantitative and interdisciplinary assessments of the deposits and impacts of the PDCs on the population, buildings, vegetation and infrastructure and in this paper we have described our methodologies and preliminary findings. Remote sensing data, in particular high-resolution satellite imagery and media images taken during rescue operations, provided a new dimension to the impact assessment and were invaluable in mapping deposits and damage across the large impact areas and also chronologically through the eruption. Detailed scientific ground-truthed observations of eruption processes and impacts that can support satellite imagery are difficult to obtain in multi-stage eruptions; however, for the Merapi 2010 eruption media images and eyewitness accounts of the eruption provided key impact data that could be used to assist and inform detailed field studies, making the impact assessment the first of its kind. Through analysis of remote sensing data, eyewitness, community and scientific accounts of the eruption, as well as comprehensive field studies, we have been able to catalogue and map the eruptive deposits and their impacts in great detail. This has allowed us to constrain PDC impact dynamics, better informing the relationship between process and impact and therefore estimates of physical vulnerability to PDCs.

Our interdisciplinary approach, where geological, engineering and medical studies were carried out in parallel in the same study areas enabled us very shortly after the disaster to interpret and reconstruct the PDC impact dynamics, timing and chronology with the best available data and in an integrated manner that has not been feasible before. Such a comprehensive assessment could not have been achieved by one discipline alone; for example, in Bronggang village, approximately 13.5 km from source, geological investigations identified that the village was impacted by a number of separate PDCs over a short period (minutes), which had important implications for our

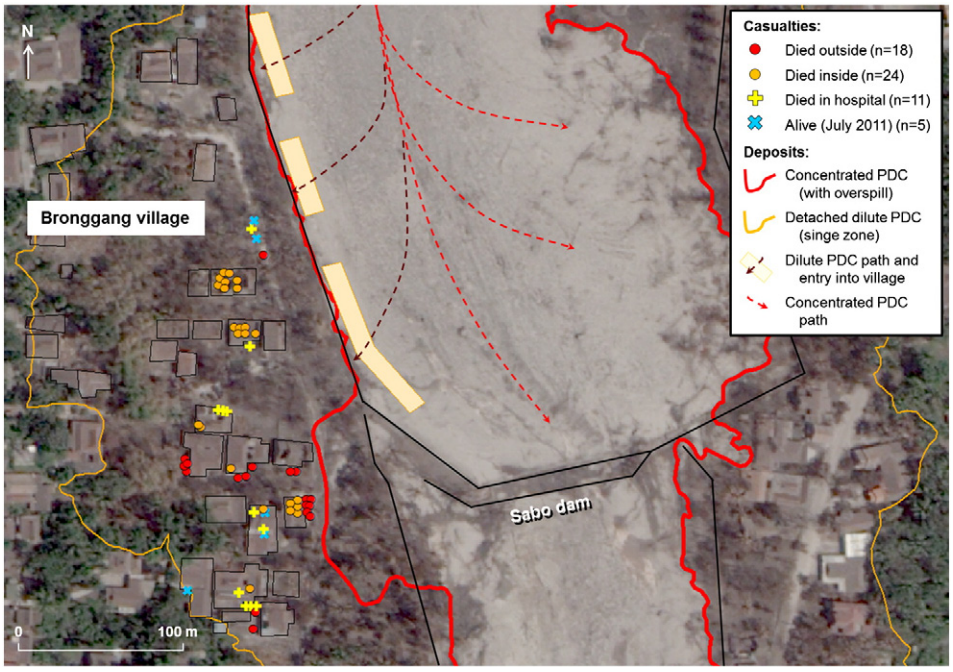

Fig. 9. Casualty locations and types in Bronggang village, approximately 13.5 km from the vent. From eyewitness accounts we know that some of those who died outside were struck while inside their homes and presumably vice versa. Overspill concentrated PDC lobes and a number of dilute, low temperature (200–300 °C) and low pressure (<1 kPa) PDCs detached from their parent channelised PDCs in the Gendol river as a result of changes in the valley morphology (a bend in the river towards the east and constriction of the channel by a Sabo dam) and entered the village at approximately 00:15 local time (UTC + 7 h) on 5 November killing or fatally injuring 51 people who were in the process of evacuating. The location of Bronggang village is shown in Fig. 1a. Digital Globe satellite image taken 10 November 2010 at 0.5 km resolution.

damage and casualty studies. Seismic records, eyewitness accounts and media images, in concert with medical data, enabled us to constrain the timing of the PDCs and the severity of casualties while damage studies examined the interior and exterior of houses to establish that dynamic pressures and temperatures associated with PDCs in Bronggang were low (<1 kPa and approximately 200–300 °C). Victims inside their homes, as well as those caught outside, died (Fig. 9) and we conclude that the building ventilation openings readily permitted the infiltration of the hot PDC. Due to the relatively low pressure and thermal impact of the surges in Bronggang it is likely that people could have survived inside buildings if they had been well sealed. Most burnt survivors who lived long enough to be taken to hospital required specialised treatment and care for their burns.

The quantitative empirical data collected as part of the ongoing forensic studies discussed here can be used to reconstruct the dynamics of damaging PDCs and support modelling efforts (e.g. as for Merapi: Charbonnier et al., 2013; Soufrière Hills Volcano: Esposti Ongaro et al., 2008; and Mount Saint Helens: Esposti Ongaro et al., 2012) and provide valuable hazard and vulnerability information for forecasting and making risk assessments, including modelling the consequences of explosive volcanic eruptions at Merapi and other dome-forming volcanoes (e.g. as for La Soufrière of Guadeloupe: Spence et al., 2008).

Acknowledgements

We would like to thank Estu Mei, Noer Choliq, Jochen Berger, David Damby and all colleagues at CVGHM as well as Doctors Danang Sri Hadmoko and Bambang Widjaya Hariadi of University Gadjah Mada in Yogyakarta, who were invaluable in supporting our field studies. Particular thanks are offered to the surgeons and doctors at Dr. Sardjito Hospital in Yogyakarta who donated their time to discussing the eruption crisis and providing data regarding the casualties. Our heartfelt thanks are offered to our interpreter, Teguh Hari Prasetyo, and the village chiefs and other eyewitnesses of the eruption who very generously donated their time in recounting their tragic experiences during the eruption. We are also grateful to Céline Vidal for remotely mapping pre-eruption building locations in the proximal impact area and Antonios Pomonis for valuable discussions regarding the engineering aspects of building damage. We thank the CASAVA (ANR contract ANR-09-RISK-002), MIA-VITA (EU FP7-ENV contract 211393) and VOLDIES (ERC contract 228064) projects for funding. Satellite imagery was purchased as part of the CASAVA project. Finally, we are grateful to Karim Kelfoun and an anonymous reviewer for their invaluable and detailed comments and to Philippe Jousset for his careful editing of this manuscript.

References

Abdurachman, E.K., Bourdier, J.L., Voight, B., 2000. Nuées ardentes of 22 November 1994 at Merapi volcano, Java, Indonesia. Journal of Volcanology and Geothermal Research 100 (1–4), 345–361.

Aspinall, W.P., 2006. Structured elicitation of expert judgement for probabilistic hazard and risk assessment in volcanic eruptions. In: Mader, H.M., Coles, S.G., Connor, C., Connor, L. (Eds.), Statistics in Volcanology. Geological Society for IAVCEI, London, pp. 15–30.

Baxter, P.J., 1990. Medical effects of volcanic eruptions. Bulletin of Volcanology 52 (7), 532–544.

Baxter, P.J., Boyle, R., Cole, P., Neri, A., Spence, R., Zuccaro, G., 2005. The impacts of pyroclastic surges on buildings at the eruption of the Soufrière Hills volcano, Montserrat. Bulletin of Volcanology 67 (4), 292–313.

Baxter, P.J., Aspinall, W.P., Neri, A., Zuccaro, G., Spence, R.J.S., Cioni, R., Woo, G., 2008. Emergency planning and mitigation at Vesuvius: a new evidence-based approach. Journal of Volcanology and Geothermal Research 178 (3), 454–473.

Belousov, A., Voight, B., Belousova, M., 2007. Directed blasts and blast-generated pyroclastic density currents: a comparison of the Bezymianny 1956, Mount St Helens 1980, and Soufrière Hills, Montserrat 1997 eruptions and deposits. Bulletin of Volcanology 69 (7), 701–740.

Boston.com, 2010. Images available from the authors and at http://www.boston.com/bigpicture/2010/11/mount_merapis_eruptions.html (Last accessed 05/12/12).

BSI, 1997. Loading for Buildings. Part 2: Code of practice for wind loads. British Standards Institution BS6399-2, p. 115.

Budi-Santoso, A., Lesage, P., Dwiyono, S., Sumarti, S., Subrandriyo, Surono, Jousset, P., Metaxian, J.-P., 2013. Analysis of the seismic activity associated with the 2010 eruption of Merapi Volcano, Java. Journal of Volcanology and Geothermal Research. 261 (1), 153–170.

Bulletin of the Global Volcanism Network, 2011. BGVN 36:1–2. Merapi: Eruption started 26 October 2010; 386 deaths more than 300,000 evacuated.

CASAVA project, 2010–2013. Understanding and assessing volcanic hazards, scenarios, and risks in the Lesser Antilles: Implications for decision-making, crisis management, and pragmatic development. https://sites.google.com/site/casavaanr.
Charbonnier, S.J., Gertisser, R., 2008. Field observations and surface characteristics of pristine block-and-ash flow deposits from the 2006 eruption of Merapi Volcano, Java, Indonesia. Journal of Volcanology and Geothermal Research 177 (4), 971–982.
Charbonnier, S.J., Germa, A., Connor, C.B., Gertisser, R., Preece, K., Komorowski, J.-C., Lavigne, F., Dixon, T., Connor, L., 2013. Evaluation of the impact of the 2010 pyroclastic density currents at Merapi volcano from high-resolution satellite imagery, field investigations and numerical simulati. Journal of Volcanology and Geothermal Research. 261 (1), 295–315.
Clarke, A.B., Voight, B., 2000. Pyroclastic current dynamic pressure from aerodynamics of tree or pole blow-down. Journal of Volcanology and Geothermal Research 100 (1–4), 395–412.
EERI, 2006. The Mw 6.3 Java, Indonesia, earthquake of May 27, 2006.
Esposti Ongaro, T., Clarke, A.B., Neri, A., Voight, B., Widiwijayanti, C., 2008. Fluid dynamics of the 1997 Boxing Day volcanic blast on Montserrat, West Indies. Journal of Geophysical Research 113 (B3), B03211.
Esposti Ongaro, T., Clarke, A.B., Voight, B., Neri, A., Widiwijayanti, C., 2012. Multiphase flow dynamics of pyroclastic density currents during the May 18, 1980 lateral blast of Mount St. Helens. Journal of Geophysical Research 117 (B6), B06208.
Hendry, A.W., Sinha, B.P., Davies, S.R., 1997. Design of masonry structures. Taylor & Francis.
Indonesian National Disaster Management Agency (BNPB), 2010. Data korban erupsi Gunung Merapi (12 December).
Jousset, P., Budi-Santoso, A., Jolly, A.D., Surono, Boichu, M., Dwiyono, S., Sumarti, S., Hidayati, S., Thierry, P., 2013. Signs of magma ascent in LP and VLP seismic events and link to degassing: An example from the 2010 explosive eruption at Merapi volcano, Indonesia. Journal of Volcanology and Geothermal Research. 261 (1), 171–192.
Kelfoun, K., Legros, F., Gourgaud, A., 2000. A statistical study of trees damaged by the 22 November 1994 eruption of Merapi volcano (Java, Indonesia): relationships between ash-cloud surges and block-and-ash flows. Journal of Volcanology and Geothermal Research 100 (1–4), 379–393.
Kennan, G., 1902. The tragedy of Pelée. The Outlook Company, New York (257 pp.).
Komorowski, J.-C., Jenkins, S., Baxter, P.J., Picquout, A., Lavigne, F., Charbonnier, S., Gertisser, R., Preece, K., Cholik, N., Budi-Santoso, A., Surono, 2013. Paroxysmal dome explosion during the Merapi 2010 eruption: Processes and facies relationships of associated high-energy pyroclastic density currents. Journal of Volcanology and Geothermal Research 261 (1), 260–294 Special Issue: Merapi eruption.
Lacroix, A., 1904. La Montagne Pelée et ses eruptions. Masson, Paris (650 pp.).
Lavigne, F., Komorowski, J.C., Jenkins, S., Baxter, P., Vidal, C., Mei, E.T.W., Picquout, A., Grancher, D., Brunstein, D., N. C., 2011. Satellite Remote-sensing and Field Analysis of Casualties and Damage Caused by the 2010 eruption of Merapi Volcano Indonesia. Remote sensing, natural hazards and environmental change, Singapore.
Lipman, P., Mullineaux, D.R. (Eds.), 1981. The 1980 Eruptions of Mount St. Helens, Washington (1–844 pp.).
MIA-VITA project, 2009–2012. MItigate and Assess risk from Volcanic Impact on Terrain and human Activities. http://miavita.brgm.fr.
SAFER project, 2006–2009. Seismic eArly warning For EuRope. http://www.saferproject.net/.
Sparks, R.S.J., Barclay, J., Calder, E.S., Herd, R.A., Komorowski, J.-C., Luckett, R., Norton, G.E., Ritchie, L.J., Voight, B., Woods, A., 2002. Generation of a debris avalanche and violent pyroclastic density current on 26 December (Boxing Day) 1997 at Soufrière Hills Volcano, Montserrat. In: Druitt, T.H., Kokelaar, B.P. (Eds.), The eruption of Soufrière Hills Volcano, Montserrat, from 1995 to 1999. Geological Society, London, pp. 409–434.
Spence, R.J.S., Baxter, P.J., Zuccaro, G., 2004. Building vulnerability and human casualty estimation for a pyroclastic flow: a model and its application to Vesuvius. Journal of Volcanology and Geothermal Research 133 (1–4), 321–343.
Spence, R., Kelman, I., Brown, A., Toyos, G., Purser, D., Baxter, P., 2007. Residential building and occupant vulnerability to pyroclastic density currents in explosive eruptions. Natural Hazards and Earth Systems Sciences 7, 219–230.
Spence, R., Komorowski, J.-C., Saito, K., Brown, A., Pomonis, A., Toyos, G., Baxter, P., 2008. Modelling the impact of a hypothetical sub-Plinian eruption at La Soufrière of Guadeloupe (Lesser Antilles). Journal of Volcanology and Geothermal Research 178 (3), 516–528.
Surono, Jousset, P., Pallister, J., Boichu, M., Buongiorno, M.F., Budi-Santoso, A., Costa, F., Andreastuti, S., Prata, F., Schneider, D., Clarisse, L., Humaida, H., Sumarti, S., Bignami, C., Griswold, J., Carn, S., Oppenheimer, C., Lavigne, F., 2012. The 2010 explosive eruption of Java's Merapi volcano — a '100-year' event. Journal of Volcanology and Geothermal Research 241–242, 121–135.
Tanguy, J.-C., 1994. The 1902–1905 eruptions of Montagne Pelée, Martinique: anatomy and retrospection. Journal of Volcanology and Geothermal Research 60 (2), 87–107.
Taylor, G.A.M., 1958. The 1951 Eruption of Mount Lamington, Papua. Australian Department of National Developments, Bureau of Mineral Resources, Geology and Geophysics, Canberra.
Thouret, J.-C., Lavigne, F., Kelfoun, K., Bronto, S., 2000. Toward a revised hazard assessment at Merapi volcano, Central Java. Journal of Volcanology and Geothermal Research 100 (1–4), 479–502.
TNO, 1992. Methods for the determination of possible damage to people and objects resulting from the release of hazardous materials. CPR16E (The Green Book), Netherlands.
Voight, B., Davis, M.J., 2000. Emplacement temperatures of the November 22, 1994 nuée ardente deposits, Merapi Volcano, Java. Journal of Volcanology and Geothermal Research 100 (1–4), 371–377.
Voight, B., Constantine, E.K., Siswowidjoyo, S., Torley, R., 2000. Historical eruptions of Merapi Volcano, Central Java, Indonesia, 1768–1998. Journal of Volcanology and Geothermal Research 100 (1–4), 69–138.
Wills, J.A.B., Lee, B.E., Wyatt, T.A., 2002. A model of wind-borne debris damage. Journal of Wind Engineering and Industrial Aerodynamics 90 (4–5), 555–565.
Wilson, T., Kaye, G., Stewart, C., Cole, J., 2007. Impacts of the 2006 Eruption of Merapi volcano, Indonesia, on Agriculture and Infrastructure. GNS Science Report 2007/07.